

A Case Study on the Comparison of Non-parametric Spectrum Methods for Broken Rotor Bar Fault Detection

Bulent Ayhan, Mo-Yuen Chow, H. Joel Trussell
Advanced Diagnosis and Control Lab
Department of Electrical and Computer Engineering
North Carolina State University
Raleigh, NC 27695, USA
bayhan@unity.ncsu.edu, chow@eos.ncsu.edu, hjt@eos.ncsu.edu

Myung-Hyun Song
Department of Electrical Control Engineering
Sunchon University
315 Maegokdong Sunchon
Cheonnam Korea
mhsong@sunchon.ac.kr

Abstract – Broken rotor bars in an induction motor create asymmetries and result in abnormal amplitude of the sidebands around the fundamental supply frequency and its harmonics. Applying a spectrum analysis technique on motor current and inspecting the spectrum amplitudes at the broken rotor bar specific frequencies for abnormality is a well-known procedure for broken rotor bar fault detection and diagnosis. Among the spectrum analysis techniques for broken rotor bar fault detection, the Fast Fourier Transform (FFT) is the most widely used technique. There are other spectrum techniques, which are based on the power spectral density estimates. In this paper we compare the three well-known spectrum analysis methods: FFT, periodogram and Welch's periodogram methods according to their performance on the broken rotor bar fault detection problem. The results indicate that Welch's periodogram method has better fault discrimination capability and is more robust compared to the other two methods. A statistical hypothesis test applied to the results of the three methods depicts the comparison results quantitatively.

I. INTRODUCTION

Induction motors have dominated the field of electromechanical energy conversion by having 80% of the motors in use [1], [2]. The applications of induction motors are widespread. Some are key elements in assuring the continuity of the process and production chains of many industries. The list of the industries and applications that they take place in is rather long. A majority are used in electric utility industries, mining industries, petrochemical industries, and domestic appliances industries. Induction motors are often used in hostile environments and critical applications such as nuclear plants, aerospace and military applications, where the reliability must be at high standards.

The failure of induction motors can result in a total loss of the machine itself, in addition to a likely costly downtime of the whole plant. More important, these failures may even result in the loss of lives, which cannot be tolerated. Thus, condition monitoring techniques to prevent induction motor failures are of great concern in industry and are gaining increasing attention [3]-[7].

Induction motors often operate in hostile environments such as corrosive and dusty places. They are also exposed to a variety of undesirable conditions and situations such as misoperations. These unwanted conditions can cause the induction motor to go into a premature failure period, which may result in an unserviceable condition of the motor, if not detected at its early stages of the failure period. The early detection of the incipient motor fault is thus of great concern. Rotor failures are among these failures and they now account

for the 5-10% of total induction motor failures [8]. Since 1980, the broken rotor bar fault detection problem has created substantial interest among researchers [9], [10]. Several monitoring techniques have been developed, most of which are based on motor current signature analysis (MCSA) [11]. In recent years, several advanced signal processing techniques such as High Resolution Spectral Analysis, Higher Order Statistics and Wavelet Analysis have been applied to this fault detection problem [1], [10], [12], [13].

MCSA techniques include parametric and non-parametric spectrum analysis methods of motor current in general. The most widely used non-parametric spectrum method is the well-known Fast Fourier Transform (FFT). FFT yields efficient and reasonable results, which makes it a powerful tool as a MCSA technique.

Power Spectral Density (PSD) analysis of motor current, which is also FFT-based, is another widely used MCSA technique. There are several approaches to calculate PSD estimates. Periodogram method, which is known as the classical way to estimate PSD, is one of these ways.

Welch's periodogram is another way to calculate PSD estimates, which is also an FFT-based method. This method differs from the classical periodogram by splitting the data into segments. It then calculates the periodogram of each windowed segment and takes the average of the periodograms to find the final PSD estimate. These methods will be further discussed in the later sections.

The aim of this paper is to present a comparison of these three spectrum analysis methods on the fault detection performance of broken rotor bar in induction motors. The induction motor data used in this study is collected through an actual experiment setup in a laboratory environment. The fault detection performance comparison of the three investigated spectrum methods has been carried out at different motor load conditions and at different broken rotor bar fault specific frequencies. The spectrum amplitudes of healthy and faulty motor data resulting from each method are examined statistically in order to find the most efficient spectrum method. We then use a hypothesis test based on the t-test P-value to draw a statistically significant conclusion about the performance order of the three methods.

This paper is organized as follows: Section II discusses the frequencies of interest to the broken rotor bar problem. Section III describes the fundamental properties of the three spectrum analysis methods. Section IV presents the experiment setup and motor data specifications. The experimental results and statistical analysis are described in Section V. Finally, Section VI presents conclusions.

II. MOTOR CURRENT SPECTRAL COMPONENTS FOR BROKEN ROTOR BAR

Kliman, Thomson, Filipetti, Elkasabgy [14]-[17] used motor current signature analysis (MCSA) methods to detect broken rotor bar faults by investigating the sideband components around the supplied current fundamental frequency (i.e. line frequency), f_o :

$$f_b = (1 \pm 2s)f_o, \quad (1)$$

where f_b are the sideband frequencies associated with the broken rotor bar, s is the per unit motor slip. The slip s is defined as the relative mechanical speed of the motor, n_m with respect to the motor synchronous speed, n_s , as:

$$s = \frac{n_s - n_m}{n_s}. \quad (2)$$

The motor synchronous speed, n_s , is related to the line frequency f_o as:

$$n_s = \frac{120f_o}{P}, \quad (3)$$

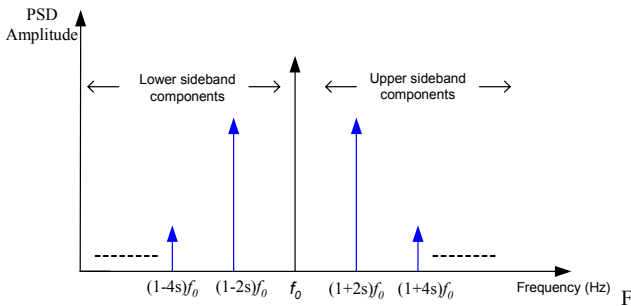
where P is the number of poles of the motor and constant '120' is used to express the motor synchronous speed, n_s , in revolutions per minute (rpm) unit.

The lower sideband frequency component $f_b = (1-2s)f_o$ is specifically due to the broken rotor bar; the upper sideband frequency component $f_b = (1+2s)f_o$ is due to the consequent speed oscillation [9].

The broken bars also give rise to a sequence of other sidebands given by [16]:

$$f_b = (1 \pm 2ks)f_o, \quad k = 1, 2, \dots, k_n \text{ where } f_b > 0 \quad \forall k, \quad (4)$$

and is depicted conceptually in Fig. 1.



ig. 1. Sideband frequencies around the fundamental line frequency.

Fig. 1 shows the frequency components specific to broken rotor bar fault, which is given in equation (4) for $k = 1$ and 2. These frequencies are located around the fundamental line frequency and called as lower sideband and upper sideband components.

There are other spectral components that can be observed in the stator line current due to broken rotor bar fault [14]:

$$f_b = \left[\left(\frac{k}{p} \right) (1-s) \pm s \right] f_o, \text{ where } k/p = 1, 3, 5, \dots \quad (5)$$

III. SPECTRUM ANALYSIS METHODS FOR BROKEN ROTOR BAR FAULT DETECTION

MCSA techniques used for broken rotor bar fault detection in induction motors include non-parametric spectrum analysis methods. Among these non-parametric spectrum analysis methods FFT is the most widely known and applied method. PSD analysis is another referred method that is extended from FFT. There are several different methods such as periodogram and Welch's periodogram to compute PSD. In this section we will briefly describe the general principles of FFT, periodogram and Welch's periodogram methods.

A. Fast Fourier Transform (FFT)

FFT is an algorithm to compute the Discrete Fourier Transform (DFT) of a discrete time series function with minimum computational effort. This widely used spectrum analysis method became well known after the publication of Cooley and Tukey's paper in Mathematics of Computation Journal in 1965 [18]. FFT algorithms compute the DFT of the given time series by successively decomposing the N -point DFT computation into computations of smaller size. These decompositions result in significant decrease in computational complexity if they are carried out properly [18]. To review the basics of the DFT, consider a sequence of N equispaced samples of a finite discrete time series signal, $x[n]$, defined for $0 \leq n \leq N-1$. The Discrete-Time Fourier Transform (DTFT) of $x[n]$, is a representation of this sequence in terms of a complex exponential sequence $\{e^{-j\omega n}\}$, where ω is the real frequency variable and is depicted as $X(e^{j\omega})$. $X(e^{j\omega})$ is defined as:

$$X(e^{j\omega}) = \sum_{n=0}^{N-1} x[n] e^{-j\omega n}. \quad (6)$$

The relation between $x[n]$ and its DTFT, $X(e^{j\omega})$, is derived by uniformly sampling the $X(e^{j\omega})$ on the ω -axis between $0 \leq \omega \leq 2\pi$ at $\omega_k = 2\pi k / N$, $0 \leq k \leq N-1$:

$$X(e^{j\omega}) \Big|_{\omega=2\pi k/N} = \sum_{n=0}^{N-1} x[n] e^{-j\omega n}, \quad 0 \leq k \leq N-1. \quad (7)$$

The DFT of $x[n]$, $X[k]$, is a finite length sequence obtained from $X[k] = X(e^{j\omega}) \Big|_{\omega=2\pi k/N}$, where $0 \leq k \leq N-1$.

The DFT calculation of the sequence $x[n]$ requires N^2 operations. The main idea behind FFT algorithm is to reduce the computational cost by choosing a highly composite number for N and decomposing the N -point DFT computations into smaller sizes. It is also shown that special computational advantage can be obtained by choosing N as $N = 2^m$, where m is an integer. The computational cost then reduces to $N \log_2 N$ [18].

B. Periodogram Method

The periodogram method is a way to estimate power spectrum and it is based on DFT. Let $x[n]$ be a discrete time signal, which is obtained by sampling a continuous time signal $x(t)$, $x[n] = x(nT)$, where T is the sampling interval. According to Wiener-Khintchine theorem [19], the power spectral density estimate of $x[n]$ at frequency f , $P_{xx}(f)$, can be defined as the Discrete Time Fourier Transform (DTFT) of the autocorrelation function of $x[n]$, $r_{xx}[k]$, and is shown in equation (8):

$$P_{xx}(f) = T \sum_{k=-\infty}^{\infty} r_{xx}[k] e^{-j2\pi f k T}. \quad (8)$$

The autocorrelation function of $x[n]$, $r_{xx}[k]$, can be calculated by equation (9):

$$r_{xx}[k] = E \left[x[n+k] x^*[n] \right], \quad (9)$$

where $x^*[n]$ is the complex conjugate of $x[n]$ and E is the expectation operator. If equation (9) is substituted into equation (8), the periodogram PSD estimate is found as:

$$P_{xx}(f) = \frac{1}{N} |X(f)|^2, \quad (10)$$

where $X(f)$ is the DFT of $x[n]$.

C. Welch's Periodogram Method

In Welch's Periodogram method, the data sequence, $x[n]$, $\{x[0], x[1], \dots, x[N-1]\}$, is first partitioned into K segments. The length of each segment consists of L samples and these segments can be overlapping on each other with $(L - S)$ overlapping samples, where S is the number of points to shift between segments.

Segment 1: $x[0], x[1], \dots, x[L-1]$

Segment 2: $x[S], x[S+1], \dots, x[L+S-1]$

⋮

Segment K : $x[N-L], x[N-L+1], \dots, x[N-1]$.

The weighted k^{th} segment will consist of the samples,

$$x^k[n] = w[n] x[n + kS], \text{ for } 0 \leq n \leq L-1, 0 \leq k \leq K-1, \quad (11)$$

where $w[n]$ is the window function applied to the data at each segment before the computation of the segment periodogram. The sample spectrum of the weighted k^{th} segment is depicted over the frequency range $-1/2T \leq f \leq 1/2T$ as,

$$P_{xx}^k(f) = \frac{1}{ULT} X^P(f) [X^P(f)]^* = \frac{1}{ULT} |X^P(f)|^2, \quad (12)$$

where U is the discrete time window energy,

$$U = T \sum_{n=0}^{L-1} w^2[n], \quad (13)$$

and $X^P(f)$ is the DTFT of the k^{th} segment,

$$X^P(f) = T \sum_{n=0}^{L-1} x^{(k)}[n] e^{-j2\pi f n T}. \quad (14)$$

Finally, Welch's PSD estimate has been found by averaging the periodogram values of the K segments,

$$\hat{P}_W(f) = \frac{1}{K} \sum_{k=0}^{K-1} P_{xx}^k(f). \quad (15)$$

The factor U is noted to remove the effect of the window energy bias in the PSD estimator $\hat{P}_W(f)$ [20].

IV. EXPERIMENT SETUP AND MOTOR DATA SPECIFICATIONS

In order to compare the fault detection performance of the three investigated spectrum analysis methods, we performed invasive experiments on an actual induction motor. The characteristics of the 3-phase induction motor used in our experiment are listed in Table I. The motor was tested with the healthy rotor and with the faulty rotor that had one broken rotor bar. The broken rotor bar fault was induced by filling one of the rotor bars full with anchoring cement before the die-casting process. Anchoring cement is a high strength, fast-setting gypsum cement with low conductivity. The overall data collection scheme and the actual experiment setup picture are depicted in Fig. 2 and 3 respectively.

TABLE I. INDUCTION MOTOR CHARACTERISTICS USED IN THE EXPERIMENT.

Description	Value
Power	0.75 kW (1Hp)
Input Voltage	380 V
Full Load Current	2.2 A
Supply Frequency	60 Hz
Number of Poles	4
Number of Rotor Slots	44
Number of Stator Slots	36
Full Load Torque	0.43 kg.m
Full Load Speed	1690 rpm

The induction motor was fed through a 3 phase ABB, ACS 501 inverter. A Tektronix TM 5003 current amplifier amplifies the induction motor stator currents before being sent to the interfacing Pentium PC through the oscilloscope. The needed load condition of the induction motor was established by connecting the test motor to a DC Motor, which is used as a generator and is capable of simulating any desired load condition. The speed of the induction motor was measured by a digital stroboscope.

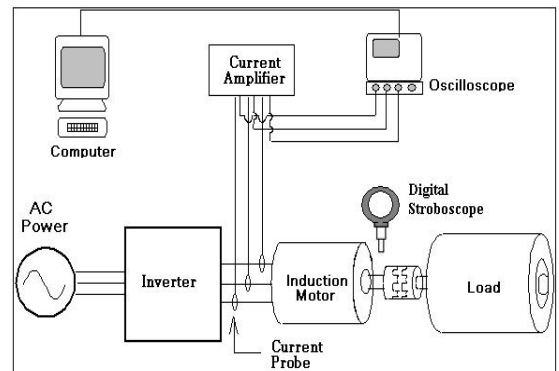


Fig. 2. Motor data collection scheme.



Fig. 3. Actual experiment setup to collect healthy and faulty motor data.

The experiments involved collecting three phase stator induction motor current and speed data for four different load conditions of the motor both with one broken rotor bar fault and without any fault. The load conditions of the motor are 25%, 50%, 75% and full load respectively. These load condition percentages are determined according to the motor nameplate information given in Table I. Thus, there are a total of 8 different experiment cases. For each individual case, 20 sets of motor current data were collected. Each motor current data set contains 10,000 samples for a duration of one second, which makes the sampling frequency 10kHz.

V. DATA ANALYSIS AND HYPOTHESIS TEST

As described in Section II, broken rotor bar specific frequencies depend on motor's slip, which is a function of motor's synchronous speed and motor's actual speed. In this study, we focus on the spectrum amplitudes of the (phase-a) motor current at two main frequencies, $(1-2s)f_o$ and $(1+2s)f_o$ that are specific to broken rotor bar fault. As a further investigation, two other broken rotor bar fault specific frequencies, which are derived according to equations (4) and (5), $(1-4s)f_o$ and $(5-4s)f_o$, will also be included in the statistical test.

In this study, we use FFT, periodogram and Welch's periodogram spectrum methods and compare the fault detection performance of each method. In all the three methods, we use 5,000 data points as the FFT data window. For the Welch's periodogram method, we use a Hanning window and 50% overlapping percentage among the partitioned segments. It has been noted that the use of Hanning window and 50% overlap lead to an efficient implementation of the FFT algorithm [20]. Finding the spectrum amplitudes at the actual frequency components, f^a , which are specific to broken rotor bar fault, is important in order to make a proper decision about the existence of a fault. In order to find these frequency components, we use the experimental motor speed data and apply equation (1). However, the calculated frequency components based on actual data may not be exactly f^a due to factors such as speed measurement noises and errors. We will call these calculated frequency components as f^* . Another crucial

constraint that we encounter in finding the proper spectrum amplitudes at the actual frequency components is the frequency resolution, Δf . Since the applied spectrum methods partition the frequency axis, we only have a limited number of discrete frequency samples that correspond to the associated frequency axis. The number of frequency samples is dependent on the length of the FFT data window used. Let's depict these frequencies with the symbol f^i , where f is the frequency value at sample point i , $0 \leq i \leq N-1$, where N is the length of the applied FFT data window. Fig. 4 illustrates the associated frequency components and the frequency resolution.



Fig. 4. Broken rotor bar fault related frequency components.

The selection of the frequency sample point that is closest to the actual frequency component, f^a , is a critical step since this choice may result in a partial to a total loss of fault information. Note also that speed measurement errors may lead to an increase in the difference between the values f^a and f^* , which can cause the selection of a frequency sample point that does not properly reflect the broken rotor bar fault. A robust spectrum analysis technique, which is able to tolerate these resolution problems and measurement noises, is thus highly preferable.

In this study, we will use the same methodology in the three spectrum methods for selecting the frequency sample point in order to make a fair comparison. We select the frequency sample that is closest to the calculated frequency component, f^* . In this frequency selection, we assume that the difference between actual frequency component, f^a and calculated frequency component, f^* is small compared to the frequency resolution. To clarify the methodology, assume that the two discrete frequency samples, which are closest to f^* from left and from right, are to be at f^{i-1}, f^i respectively. In this case, we choose the frequency sample, f^b , according to:

$$f^b = \begin{cases} f^i & \text{if } |f^i - f^*| \leq |f^{i-1} - f^*|, \\ f^{i-1} & \text{otherwise.} \end{cases} \quad (16)$$

The investigated spectrum methods are applied to both the healthy and faulty (phase-a) motor current data, which was collected while the motor was operating under different load conditions. In all the three spectrum methods, frequency sample selection is done according to equation (16). The spectrum estimates distributions of the three methods, are

depicted in Fig. 5 and 6. These spectrum estimates correspond to the broken rotor bar specific frequency components $(1+2s)f_o$ and $(1-2s)f_o$ respectively under full load condition of the motor.

Fig. 5 depicts the spectrum estimates of the three investigated methods at the frequency component $(1+2s)f_o$. In this figure, the symbol ‘o’ stands for the healthy motor spectrum estimate, while the symbol ‘x’ stands for the faulty motor spectrum estimate. Likewise, Fig. 6 depicts the spectrum estimates at the frequency component $(1-2s)f_o$.

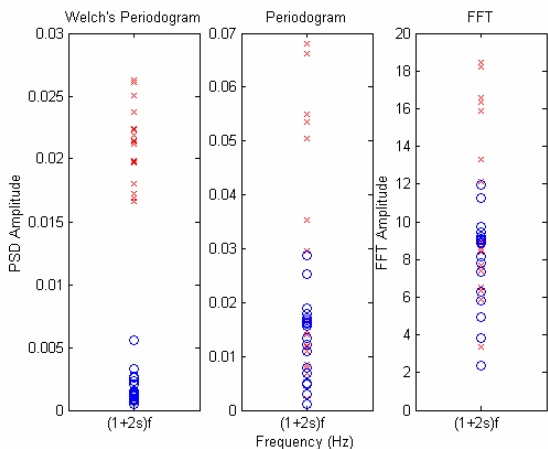


Fig. 5. Spectrum estimates of the three methods at $(1+2s)f_o$.

Fig. 5 and 6 correspond to the full load condition of the motor. However, in the statistical analysis part to be introduced next, other motor load conditions as well as two other frequency components specific to broken rotor bar fault will be investigated.

When Fig. 5 and 6 are examined from a visual perspective, it is observed that Welch’s periodogram method yields better fault detection performance compared to FFT and periodogram methods. In the Welch’s periodogram method, the two groups, which represent healthy and faulty data, can be distinguished visually from each other. However in the other two methods, this distinction is not clear. The results at the $(1+2s)f_o$ frequency component are more apparent to make this visual conclusion.

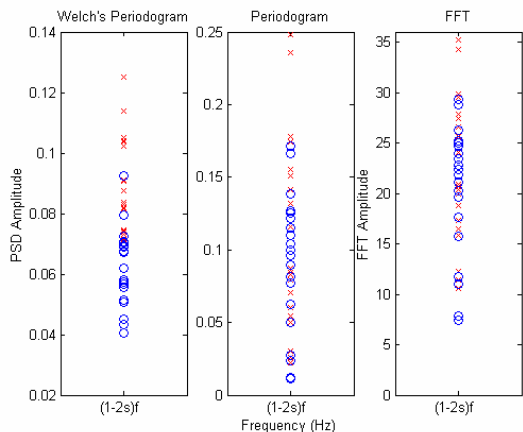


Fig. 6. Spectrum estimates of the three methods at $(1-2s)f_o$.

We will use a hypothesis test to statistically show the significant difference among the observed spectrum estimates and to make a comparison of the three spectrum methods according to their fault detection performance. The hypothesis are stated as:

H_0 : The mean of healthy motor spectrum estimates is the same as the mean of faulty motor spectrum estimates at the inspected frequency.

H_1 : The mean of healthy motor spectrum estimates is not the same as the mean of faulty motor spectrum estimates at the inspected frequency.

We apply these hypotheses on all the specific frequencies under investigation for the three spectrum methods. We then use t-test and P-value results to evaluate if the hypothesis test is significant with the spectrum data under investigation [21].

In general, the t-test allows us to assess whether the means of two groups are statistically different from each other. The t-test evaluates the means of the compared groups relative to the variability of their samples. In our case the two groups under comparison are healthy and faulty spectrum estimates under the same load condition of the motor. The numerical value that the P-value yields is a probability value, which gives information on whether the two groups differ from each other and at what degree. If P-value is smaller than a pre-defined significance level, then the null hypothesis, H_0 , is rejected. This implies that the difference between the means of the compared groups is statistically significant. Otherwise H_1 is rejected. In our analyses, we use a significance level value of 0.05, which is also interpreted as 95% confidence interval. This value is the most commonly used significance level in statistics. For further information about t-test, P-value and significance level please refer to [21]. Tables II-IV list the P-values of the three spectrum methods at the inspected frequencies under different motor load conditions. In these tables, P-values, which are lower than the determined significance level, 0.05, are highlighted. The lowest P-values, which are interpreted as providing better discrimination performance, belong to the Welch’s periodogram method. P-values of the periodogram method are also low but not as low as Welch’s method, while FFT has relatively higher P-values among the three methods under investigation.

TABLE II. FFT T-TEST P-VALUES FOR HEALTHY AND FAULTY MOTOR

	$(1-2s)f_o$	$(1+2s)f_o$	$(1-4s)f_o$	$(5-4s)f_o$
25%	0.8590196	0.5693429	0.5663659	0.01403992
50%	0.0055127	0.0000950	0.0000904	5.48108e-9
75%	0.0000471	0.0000052	0.0002166	3.5727e-20
100%	0.3749742	0.0103151	0.0000005	2.7664e-20

TABLE III. PERIODOGRAM METHOD T-TEST P-VALUES.

	$(1-2s)f_o$	$(1+2s)f_o$	$(1-4s)f_o$	$(5-4s)f_o$
25%	0.661463	0.1780966	0.1435032	0.00867367
50%	0.0035777	0.0000287	0.0008466	0.00000027
75%	0.0000265	0.0000064	0.0005782	2.6248e-15
100%	0.3163098	0.0076293	0.0000188	8.2953e-14

TABLE IV. WELCH'S PERIODOGRAM METHOD T-TEST P-VALUES.

	$(1-2s)f_o$	$(1+2s)f_o$	$(1-4s)f_o$	$(5-4s)f_o$
25%	0.091906	0.000070	4.00e-08	8.92e-10
50%	1.00e-11	2.31e-21	0.0000057	3.88e-10
75%	1.57e-22	5.53e-21	1.29e-18	8.22e-23
100%	3.80e-07	6.24e-25	6.53e-16	2.84e-28

The statistical results show that Welch's periodogram method is more efficient than FFT and periodogram methods in terms of fault detection performance. Although all the three methods are based on DFT technique, the use of a Hanning window and overlapping segments in Welch's method contribute to the fault detection performance in a positive way. The use of a Hanning window reduces the side effect of the sidelobes and this results in a decrease in the PSD estimate bias [20]. The sidelobes of the signal spectrum cause the signal power leak into other frequencies. The bias of the PSD estimate is due to this spectral leakage. Applying a tapered window to the signal in the spectral estimation, such as a Hanning window reduces this effect considerably. This results in a decreased estimation bias, which shows that the PSD estimate is closer to the real value. On the other hand, overlapping segments cause data treatment and smoothing of the PSD estimate. As the number of data segments increase, the PSD estimate variance decreases [20]. Both these positive effects suggest Welch's periodogram method is a preferred approach when compared to the other two inspected methods in broken rotor bar fault detection of induction motors.

VI. CONCLUSION

Spectrum analysis methods are among the motor current signature analysis (MCSA) techniques used for broken rotor bar fault detection and diagnosis in induction motors. This paper presents a comparison of the investigated three non-parametric spectrum methods, FFT, periodogram, Welch's periodogram on actual motor data with respect to their fault detection performance. The statistical results based on experimental motor data clearly indicate that Welch's periodogram method has better discrimination capability and is more robust compared to the other two methods. The concept of using overlapping segments and a Hanning window within the Welch's method causes an improvement in the PSD estimate. This improvement results in a decrease in the PSD estimate bias and variance values and provides a significant improvement in the fault detection performance of this method compared to the other two methods.

VII. REFERENCES

- [1] M.E.H. Benbouzid, G.B. Kliman, "What stator current processing based technique to use for induction motor rotor faults diagnosis?," IEEE Power Engineering Review, August 2002.
- [2] T.W. Wan, H. Hong, "An on-line neurofuzzy approach for detecting faults in induction motors," Electric Machines and Drives Conference, IEMDC 20001, Cambridge, MA, June 17-20, 2001, pp. 878-883.
- [3] O. V. Thursen *et al.*, "A survey of faults on induction motors in offshore oil industry, petrochemical industry, gas terminals, and oil refineries," IEEE Trans. Industry Applications, vol. 31, no. 5, September-October 1995, pp. 1186-1196.
- [4] M.E.H. Benbouzid, "Bibliography on induction motors faults detection and diagnosis," IEEE Trans. Energy Conversion, vol. 14, no. 4, December 1999, pp. 1065-1074.
- [5] B. Li., M.-Y. Chow, Y. Tipsuwan, J.C. Hung, "Neural-network-based motor rolling bearing fault diagnosis," IEEE Trans. Industrial Electronics on, vol. 47, no. 5, Oct. 2000, pp. 1060-1069.
- [6] S. Altug, M.-Y. Chow, H.J. Trussell, "Fuzzy inference systems implemented on neural architectures for motor fault detection and diagnosis," IEEE Trans. on Industrial Electronics, vol. 46, no. 6, Dec. 1999, pp. 1069-1079.
- [7] S. Altug, M.-Y. Chow, "Comparative analysis of fuzzy inference systems implemented on neural structures," International Conference on Neural Networks, 1997, vol. 1, pp. 426-431.
- [8] M. Haji, H.A. Toliyat, "Pattern recognition - a technique for induction machines rotor broken bar detection," IEEE Trans. on Energy Conversion, vol. 16, no. 4, Dec. 2001, pp. 312-317.
- [9] S. Nandi, H.A. Toliyat, "Condition monitoring and fault diagnosis of electrical machines," Industry Applications Conference, Thirty-fourth IAS Annual Meeting, vol. 1, pp. 197-204.
- [10] K. Abbaszadeh, J. Milimonfared, M. Haji, H. Toliyat, "Broken bar detection in induction motor via wavelet transformation," Twenty-seventh annual conference of the IEEE, IECON 2001, vol.1, pp. 95-99.
- [11] G.B. Kliman, J. Stein, "Methods of motor current signature analysis," Electric machines and power systems, pp. 463-474, 1992.
- [12] M.E.H. Benbouzid, M. Vieira, C. Theys, "Induction motors' faults detection and localization using stator current advanced signal processing techniques", IEEE Trans. on Power Electronics, vol. 14, no. 1, Jan. 1999, pp. 14-22.
- [13] N. Arthur *et al.*, "Induction machine condition monitoring with higher order spectra - Part I: Fundamentals and fixed frequency operation," in Proc. IEEE IECON'98, vol.3, Aachen, Germany, 1998, pp. 1889-1894.
- [14] G.B. Kliman *et al.*, "Non-invasive detection of broken rotor bars in operating induction motors", IEEE Trans. on Energy Conversion vol. EC-3, no. 4, pp. 873-879, 1988.
- [15] W.T. Thomson, I.D. Stewart, "On-line current monitoring for fault diagnosis in inverter fed induction motors", IEE Third international conference on power electronics and drives, London, pp.432-435, 1988.
- [16] F. Filipetti *et al.*, "AI Techniques in induction machines diagnosis including the speed rifle effect," IEEE- IAS Annual Meeting Conference, San Diego, pp. 655-662, Oct 6-10, 1996.
- [17] N.M. Elkasabgy, A.R. Eastham, G.E. Dawson, "Detection of broken bars in the cage rotor on an induction machine," IEEE Trans. on Industrial Applications, vol. IA-22, no. 6, pp. 165-171, Jan/Feb 1992.
- [18] J.W. Cooley, J.W. Tukey, "An algorithm for machine calculation of complex series", Mathematics of Computation Journal, 19(90), 297-301, 1965.
- [19] S.M. Kay and S.L. Marple "Spectrum Analysis- A modern perspective," Proc. IEEE, vol. 69, pp. 1380-1419, Aug. 1981.
- [20] S.L. Marple, "Digital Spectral Analysis with Applications", Prentice Hall, 1987.
- [21] D.C. Montgomery, G.C. Runger, N.F. Hubele, Engineering Statistics, John Wiley & Sons, New York, 1999.